Locally Multiaxial Fracture Behaviour of High-Strength Cold-Drawn Prestressing Steel Wires

J. Toribio[1], B. González[1] and J. C. Matos[2]

[1] Department of Materials Engineering, University of Salamanca, E.P.S. Zamora, Campus Viriato, Avda. Requejo 33, 49022 Zamora, Spain. e-mail: toribio@usal.es
[2] Department of Computing Engineering, University of Salamanca, E.P.S. Zamora, Campus Viriato, Avda. Requejo 33, 49022 Zamora, Spain. e-mail: jcmatos@usal.es

ABSTRACT. *This paper deals with the influence of the cold drawing process on the fracture behaviour of pearlitic steels. To this end, fracture test under axial loading were performed on steel wires with different drawing degree (from a hot rolled bar to a commercial prestressing steel wire), transversely pre-cracked by fatigue, analyzing in detail the changes in fracture micromechanisms. The deflection angles of the fracture path were measured by longitudinal metallographic sections and the characteristic parameters of the load-displacement plot were related to different fracture events. Results allowed a calculation of critical stress intensity factors for different fracture angles and drawing degrees, thus evaluating the strength anisotropy and obtaining a sort of directional toughness.*

INTRODUCTION

The micro-mechanisms taking place during the fracture process of metals and alloys, as well as the fracture toughness, change with the temperature, the loading rate, and the cold work [1-3]. In the particular case of pearlitic steel used to produce high-strength cold-drawn prestressing wires, the cold drawing process affects the phenomenon of the fracture, so that the most heavily drawn steels (undergoing severe plastic deformation) exhibit strength anisotropy, and a change in the crack propagation direction, which approaches the wire axis or drawing direction [4]. This leads to the calculation of two angular fracture toughness, one in the radial direction and the other in the axial one, the first being much greater than the second for steels with severe plastic deformation [5-7]. In wires with axisymmetric notches, the degree of the fracture anisotropy also depends on the notch geometry [8].

The fracture surface of pearlitic steel presents a change in the fracture mechanism as the wire is drawn [6]. While in the hot rolled wire the fracture is produced through cleavage, in the early stages of cold drawing there appears fracture caused by growth and coalescence of microvoid and then cleavage. On the other hand, the heavily drawn steels exhibit, after the propagation of microvoids in mode I, a step at about 90º followed by a mixed propagation of microvoids and cleavage [4]. The fracture behaviour of pearlitic steel depends mainly on the size of the prior austenite grain [9-11]: the smaller the size of the grain, the greater the fracture toughness. If the pearlitic steel is cold drawn, then the pearlite colony, rather than the prior austenite grain, is the critical fracture unit determining the size of the cleavage facet [12].

EXPERIMENTAL PROCEDURE

A progressively drawn pearlitic steel was used in this work: from the hot-rolled bar (not cold drawn at all) to the cold drawn wire (obtained after seven cold drawing steps and a stress-relieving treatment), as well as the intermediate steps. In order to designate the steel, a code, comprised of the letter B followed by a digit indicating the number of drawing steps applied to each one, was used. The degree of cold drawing is characterised by means of the cumulative plastic strain ε^{P} as a function of the diameter reduction according to the following expression (Eq. 1),

$$\varepsilon^{\mathrm{p}} = \ln \frac{D_0}{D_{\mathrm{i}}} \tag{1}$$

where D_{i} is the diameter of the wire after i drawing steps and D_0 that corresponding to the initial steel before cold drawing.

To perform the fracture tests, samples of 300 mm were taken from the wires, with diameters of 12 mm in the hot rolled bar and 7 mm in the cold drawn wire. After axial tensile fatigue with a sinusoidal wave (at a frequency of 10 Hz and R-ratio equal to 0) under load control and decreasing loading steps, specimens were subjected to monotonic tensile loading under displacement control up to fracture, the crosshead speed being 3 mm/min. An extensometer was placed in front of the crack mouth (symmetrically in relation to the crack faces), so that both the load applied on the sample (F) and the relative displacement by the extensometer (u) were recorded to plot the load-displacement curve F-u.

EXPERIMENTAL RESULTS

Microstructure

The drawing process produces important microstructural changes in the steel at the two basic microstructural levels of pearlitic colonies and lamellae (Fig. 1). The colonies become progressively enlarged and oriented in axial direction with cold drawing. With regard to the lamellae, they are also axially oriented after drawing and at the same time the pearlite interlamellar spacing decreases with the level of cumulative plastic strain. Therefore, the microstructure becomes progressively packed and oriented with cold drawing.

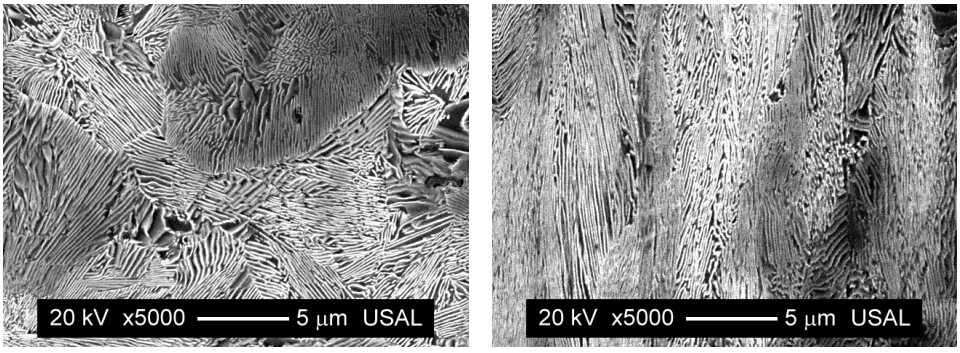

Figure 1. Microstructure, longitudinal section, B0 (left) and B7 (right).

Fracture Surface

Figure 2 shows the fracture surface from the different steels, where the fatigue surface, starting from a small mechanical cut (on the left side of the photographs), appears with a semi-elliptical final front from which the fracture initiates. Macroscopically, the fracture surfaces of the slightly drawn steels propagate perpendicularly to the applied stress, following the fatigue crack. On the contrary, in heavily drawn steels, the fracture is very anisotropic, with abundant deflections and longitudinal cracking.

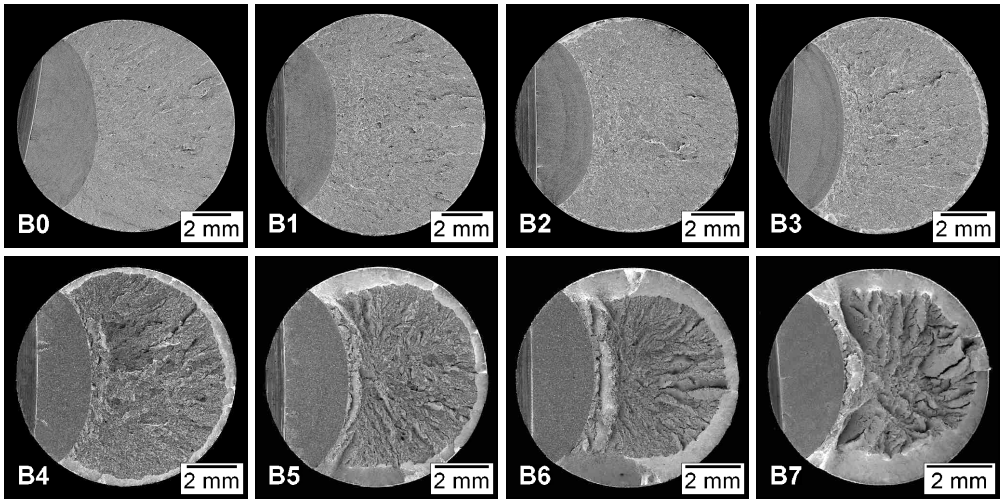

Figure 2. Fracture surfaces, B0 to B7.

Symmetrical longitudinal cuts were made in the fracture-tested specimens, they were photographed (Fig. 3), and the fracture angle was measured. In these photographs the fatigue is shown on the left, with a flatter profile, as well as the fracture appearing after such fatigue. As the plastic deformation increases with the number of drawing steps, so does the roughness of the fracture surface, as well as fracture angle with respect to the cross section of wire θ, which implies the occurrence of a fracture in *mixed mode*. Moreover, in heavily-drawn steels, at the beginning of the fracture the existence can be observed of a step at 90º with respect to the cross section of the wire.

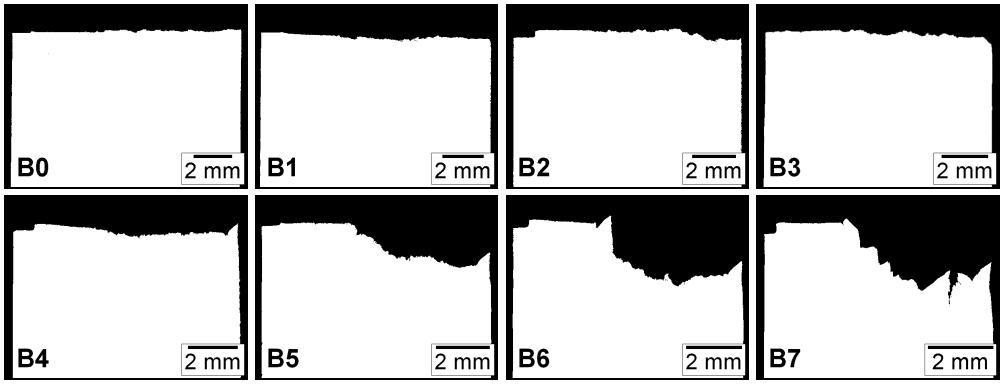

Figure 3. Longitudinal section of the fracture, B0 to B7.

Crack fronts are characterized by a semi-elliptical geometry centred on the surface of the wire. In slightly-drawn steels, a micro-void coalescence (MVC) zone appears at the fracture surface after fatigue crack, with an extension of a few tenths of a micron, whose surface increases with the cold-drawing process. Then the fracture propagates by cleavage and ends with a small external ring of MVC. The initial MVC zone was not taken into account in the calculations (due to its small size); instead of it, the crack front used in the calculations was that created by fatigue. It was modelled as a part of an ellipse of semiaxes a_f and b_f, with a_f coinciding with the crack depth.

In heavily drawn steels, the main fracture micro-mechanisms are MVC and vertical walls consisting of elongated cleavage. Such walls appear surrounding the fatigue in the form of abundant secondary radial cracking and their size increase in extension with cold drawing. The final external ring of MVC has a greater surface than in slightly drawn steels. The growth area prior to the vertical wall has a size on the order of hundreds of microns and was taken into account in the calculations, resulting in the appearance of two critical crack sizes during the fracture: the fatigue crack with semiaxes a_f and b_f, and the crack existing at the time of growth of the vertical wall by cleavage (with semiaxes a_e and b_e).

Load-Displacement Curve

The records obtained for the load-displacement curve *F-u* are different for slightly- and heavily-drawn steels (Fig. 4). Both have an initial linear zone that becomes a curve, with this curvature being generally greater as the drawing process increases, although it could also depend on other factors. The curves were characterized from two parameters: the load at the end of the linear behaviour portion of the curve (F_e) and the maximum load (F_{max}). In the heavily drawn steels, a characteristic load (F_Y) also appears that can be associated with a micro-tearing phenomenon called *pop-in* [13], which is accompanied by a characteristic tearing noise. By performing interrupted tests [14], it has been observed that the phenomenon of *pop-in* is physically associated with the occurrence of vertical cracking.

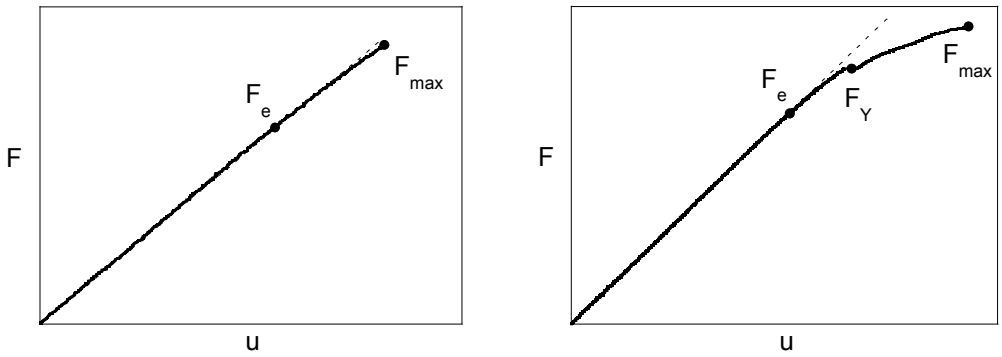

Figure 4. Load-displacement curve, B0 (left) and B7 (right).

Fracture Toughness

The value of the critical stress intensity factor SIF obtained for cracked cylindrical specimens is the fracture toughness of the material, being independent from the wire's diameter and from the crack size [15]. Once the fracture tests were carried out, the critical SIF corresponding to the

macroscopic angle of the fracture surface ($K_{IC\theta}$) was calculated, as well as the critical SIF associated with the *pop-in* phenomenon ($K_{IC90º}$) for those steels where a vertical step existed. To calculate these characteristic values, the maximum SIF was considered over practically the whole crack front in which plane strain conditions occur (the point at the wire surface was not taken into account in the calculations of the characteristic SIF).

The dimensionless SIF used in the computations is that proposed by Shin and Cai [16] in the form of a three-parameter expression (Eq. 2) as a function of the crack depth a/D, the crack aspect ratio a/b and the position along of the crack front x/h,

$$K_{I0^\circ} = K_{I0^\circ}(F,a,b) = Y\left(\frac{a}{D},\frac{a}{b},\frac{x}{h}\right)\sigma\sqrt{\pi a} \tag{2}$$

To obtain the SIF of a secondary crack with angle θ from another main one (Fig. 5), it has been considered that the local SIFs at the tip of a secondary crack (k_1^*, k_2^*) are related with the global SIFs from the main crack (K_I, K_{II}) for the case in which the secondary crack length tends to zero [17].

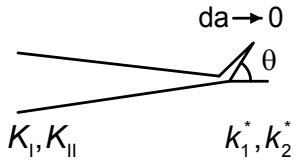

Figure 5. Crack tip deflection.

The expression of the local SIFs, for the crack tip in deflection, is shown in Eq. 3:

$$\begin{pmatrix} k_1^* \\ k_2^* \end{pmatrix} = \begin{pmatrix} K_{11} & K_{12} \\ K_{21} & K_{22} \end{pmatrix} \begin{pmatrix} K_I \\ K_{II} \end{pmatrix} \tag{3}$$

where the coefficients K_{ij} only depend on the value of the deflection angle θ. For the calculations, the coefficients obtained by Amestoy [17] were used, fitted to third-order polynomial expressions with high regression coefficients.

The energy release rate value satisfies Eq. 4:

$$G = \frac{(k_1^{*2} + k_2^{*2})}{E'} \tag{4}$$

where $E'=E/(1-\nu^2)$ in plane strain and $E'=E$ in plane stress.

In the matter of the materials that exhibit an anisotropic fracture behaviour, fracture specific energy depends on the angle of propagation, θ, with respect to the crack plane (contained in the wire cross section). The directional energy release rate, $G(\theta)$, can be related to the energy release rate at 0º, $G(0º)$, and similarly their critical values, through Eq. 5,

$$G(\theta) = (K_{11}^2 + K_{21}^2)G(0^\circ) \tag{5}$$

For the slightly drawn steels, Eq. 6 allows the calculation of the directional fracture toughness, keeping in mind the maximum load and the size of the fatigue crack,

$$K_{I\theta} = \sqrt{K_{11}^2 + K_{21}^2} K_{I0^\circ}(F_{max}, a_f, b_f) \tag{6}$$

In heavily drawn steels, the critical SIF was calculated in mode I at 90º, from the *pop-in* load. In the fracture step, corresponding to the vertical cleavage burst (Fig. 6), the relationship between the energy release rate in the axial direction (for the 90º angle) and in the radial direction (for 0º) [6, 7, 17] permits the calculation of the critical SIF at 90º from Eq. 7:

$$K_{I90^\circ} = \sqrt{0.2615} K_{I0^\circ}(F_Y, a_e, b_e) \tag{7}$$

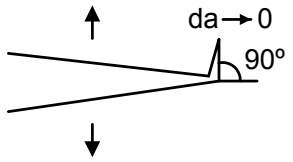

Figure 6. Crack tip deflection towards 90º.

In the crack propagation from the vertical cleavage wall, which appears in the heavily drawn steels, the energy release rate for growth in the fracture plane of angle θ can be simplified by nullifying the vertical deflection length (Fig. 7).

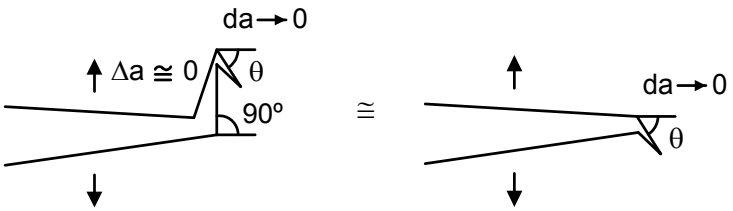

Figure 7. Crack tip deflection towards θ.

Thus, the critical SIF at θ can be calculated using Eq. 8:

$$K_{I\theta} = \sqrt{K_{11}^2 + K_{21}^2} K_{I0^\circ}(F_{max}, a_e, b_e) \tag{8}$$

Figure 8 shows the results of the critical SIF in mode I for the fracture angle θ of each drawing step, as well as those of the critical SIF in mode I for the fracture angle 90º in those steels where the anisotropy takes place in the form of vertical cracking. Both directional toughness values increase with the drawing process, but the increase of critical SIF associated with the θ angle is much more pronounced than that of the 90º angle, the former reaching values as high as 110 $MPam^{1/2}$.

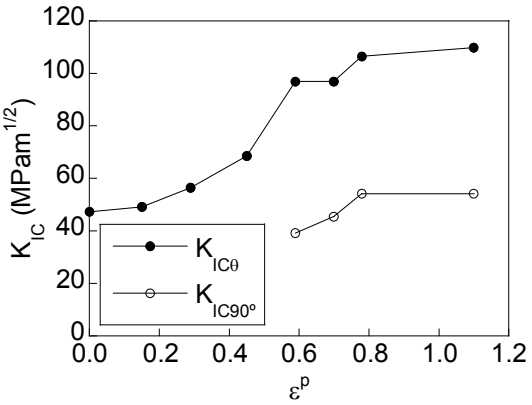

Figure 8. Fracture toughness, $K_{IC\theta}$ and K_{IC90^o}.

DISCUSSION

Cold drawing is an effective process for increasing the strength of pearlitic steel, resulting in a considerable improvement in fracture behaviour while at the same time a strong anisotropy appears during fracture, it being related to microstructural anisotropy produced by plastic deformation as a consequence of cold drawing. Figure 9 (left) shows the relationship between the fracture angle (macroscopic angle θ) and the pearlite lamellae angle (microscopic angle θ_m), both measured relative to the wire cross section, showing how both increase with plastic deformation.

The calculation of the critical SIF in mode I at 0º was carried out in a linear way when values were available for both angles. In the case that only the critical SIF for an angle other than 0º was available, the slope was not considered, because it was small. The results show that the steel becomes more anisotropic in its fracture behaviour as the number of wire drawing steps increases (Fig. 9, right). Furthermore, K_{IC0^o} increases markedly with plastic deformation, tripling itself, while K_{IC90^o} only slightly increased. For high deformations, K_{IC90^o} is significantly lower than K_{IC0^o}, which explains the presence of vertical cleavage walls on the fracture surfaces.

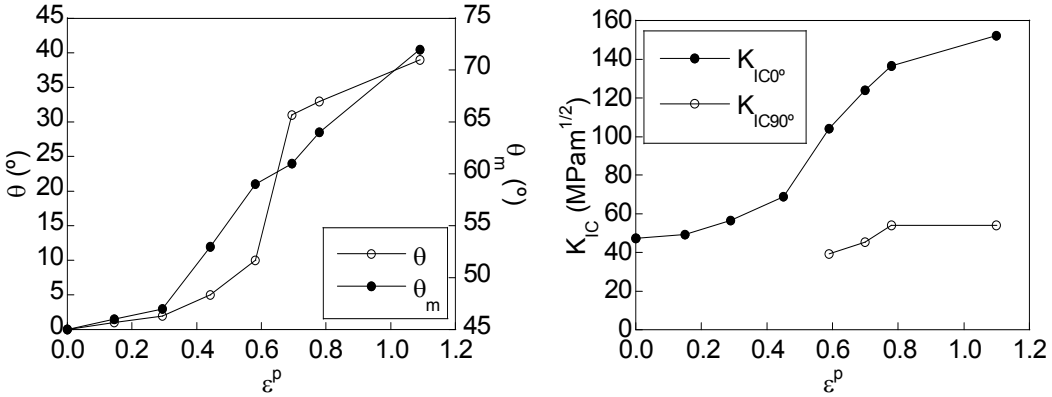

Figure 9. Fracture angle (left) and fracture toughness K_{IC0^o} and K_{IC90^o} (right).

CONCLUSIONS

Cold drawing in pearlitic steel induces strength anisotropy associated with a deflection angle in the crack path, changing from being transversal to the wire (in the non-drawn steel) to producing crack deflection with an ever increasing angle as the degree of cold drawing increases during manufacture.

The *directional toughness* (or directional critical stress intensity factor, SIF) depends on the deflection angle (macroscopic) of the fracture crack path, that angle being in turn a function of the microstructural orientation angle of the pearlite lamellae (which tend to be oriented in the wire axis or cold drawing direction).

The cold drawing process improves the fracture behaviour in mode I for a 0º angle in pearlitic steel (by increasing the fracture toughness), but it induces a marked anisotropy in its fracture behaviour (strength anisotropy, greater with increasing amount of plastic deformation after drawing) due to the strong microstructural anisotropy.

ACKNOWLEDGEMENTS

The authors acknowledge the financial support provided by the following institutions: MCYT (Grant MAT2002-01831), MEC (Grant BIA2005-08965), MICINN (Grants BIA2008-06810 and BIA2011-27870), and JCyL (Grants SA067A05, SA111A07, and SA039A08).

REFERENCES

1. Juhas, M.C., Bernstein, I.M. (1983) *Metall. Trans. A* **14**, 1379-1388.
2. Yu, S.R., Yan, Z.G., Cao, R., Chen, J.H. (2006) *Eng. Fract. Mech.* **73**, 331-347.
3. Wetscher, F., Stock, R., Pippan, R. (2007) *Mater. Sci. Eng. A* **445-446**, 237-243.
4. Toribio, J., Toledano, M. (2000) *Constr. Build. Mater.* **14**, 47-53.
5. Astiz, M.A., Valiente, A., Elices, M., Bui, H.D. (1985). In: *Life Assessment of Dynamically Loaded Materials and Structures (ECF5)*, pp. 385-396, Faria, L.O. (Ed.), EMAS, Lisbon.
6. Toribio, J., Valiente, A. (2004) *Mater. Lett.* **58**, 3514-3517.
7. Toribio, J., Valiente, A. (2006) *Eng. Fail. Anal.* **13**, 301-311.
8. Toribio, J., Ayaso, F.J. (2001) *Mater. Sci.* **37**, 707-717.
9. Alexander, D.J., Bernstein, I.M. (1982) *Metall. Trans. A* **13**, 1865-1868.
10. Park, Y.J., Bernstein, I.M. (1979) *Metall. Trans. A* **10**, 1653-1664.
11. Fernández-Vicente, A., Carsí, M., Peñalba, F., Taleff, E., Ruano, O.A. (2002) *Mater. Sci. Eng. A* **335**, 175-185.
12. Toribio, J., Ayaso, F.J. (2003) *Mater. Sci. Eng. A* **343**, 265-272.
13. Singh, U.P., Banerjee, S. (1991) *Acta Metall. Mater.* **39**, 1073-1084.
14. Toribio, J., González, B., Matos, J.C. (2007) *Int. J. Fract.* **144**, 189-196.
15. Valiente, A., Elices, M., Astiz, M.A. (1982) *Anal. Ing. Mecán.* **2**, 248-257 (in Spanish).
16. Shin, C.S., Cai, C.Q. (2004) *Int. J. Fract.* **129**, 239-264.
17. Amestoy, M., Bui, H.D., Dang-Van, K. (1981). In: *Advances in Fracture Research (ECF 5)*, pp. 107-113, Francois, D. (Ed.), Pergamon Press, Cannes.